RESEARCH ARTICLE

A Data-Driven Model Predictive Control for Wind Farm Power Maximization

MINJEONG KIM[ID]**, MINHO JANG**[ID]**, AND SUNGSU PARK**[ID]
Department of Aerospace Engineering, Sejong University, Seoul 05006, South Korea

Corresponding author: Sungsu Park (sungsu@sejong.ac.kr)

ABSTRACT This paper presents a data-driven approach to maximize the power of a wind farm by developing a dynamic mode decomposition with input and output for reduced order model (DMDior)-based reduced order model (ROM) for model predictive control (MPC). The main goal of this research is to efficiently model and manage the complex flow field within a wind farm to enhance power production. We leveraged DMDior to transform extensive high-dimensional flow data into an accurate yet simplified ROM, which successfully represents the essential dynamic features of wind flow, including the critical interactions between turbines and their adaptive response to environmental changes. Based on this ROM, the MPC framework was carefully designed. MPC uses this model to dynamically adjust the yaw angle of a wind turbine to optimally match changing wind patterns to maximize power output. The system also incorporates an adaptive Kalman filter designed for the state estimation in MPC applications. This estimation is critical to the effective execution of the MPC in each iteration. This ensures that the MPC operates based on the most up-to-date and accurate representation of the wind farm's state, improving the overall reliability and efficiency of the control strategy. This approach demonstrates a practical and effective way to increase the power output of a wind farm, with experimental results indicating a power increase of about 4.72%.

INDEX TERMS Wind farm control, data-driven approach, dynamic mode decomposition with input and output, reduced order model, model predictive control, adaptive Kalman filter.

NOMENCLATURE

ROM	Reduced Order Model.
DMD	Dynamic Mode Decomposition.
DMDior	DMD with Input and Output for Reduced-order model.
SVD	Singular Value Decomposition.
MPC	Model Predictive Control.
KF	Kalman Filter.
AKF	Adaptive Kalman Filter.
PGR	Power Growth Rate.
θ	Yaw angle of the wind turbine.
γ	Yaw offset of the wind turbine.
γ_e	Yaw error of the wind turbine.
$\dot{\gamma}$	Yaw rate of the wind turbine.

P	Electrical power of the wind turbine.
ws	Wind speed.
wd	Wind direction.
x_k	State vector of flow fields at time step k.
$\tilde{x}_k$	Reduced-order state vector of flow fields at time step k.
x_{u_k}	Previous control input vector of flow fields at time step k
x_{a_k}	Augmented state vector of flow fields at time step k.
$\hat{\tilde{x}}_k$	Estimated reduced-order sate vector of flow fields at time step k.
A, B, C, D	State-space matrices of flow fields.
$\tilde{A}, \tilde{B}, \tilde{C}$	Reduced-order state-space matrices of flow fields.
A', B', C'	Augmented state-space matrices of flow fields.

Q   State weighting matrix.

R   Control input weighting matrix.

Q_k Process noise covariance matrix at time step k.

R_k Measurement noise covariance matrix at time step k.

I. INTRODUCTION

Increasing environmental awareness and the shift to sustainable energy have made renewable energy sources, particularly wind power, crucial in the global effort to reduce greenhouse gas emissions and reliance on fossil fuels. Driven by environmental necessity and technological advances, the wind energy sector has expanded rapidly, making wind power not just an alternative to conventional energy sources, but an essential component of achieving a sustainable, low-carbon future.

The growing importance of wind energy has led to an increase in the scale of operations from individual turbines to large wind farms. These wind farms, consisting of multiple turbines, are strategically placed for optimal wind energy utilization. However, effectively managing these farms requires addressing complex aerodynamic interactions between turbines, particularly wake effects, which have a significant impact on power generation and turbine lifetime [1], [2], [3], [4], [5]. Optimizing these interactions is critical to maximizing wind farm energy production and extending turbine lifetime.

Recent research has explored optimizing wind farm control through turbine yaw angle adjustment. Yaw control, which aligns turbines to minimize wake effects, has been shown to improve overall plant efficiency and power output [6], [7], [8], [9], [10], [11], [12]. Studies have demonstrated that positive yaw misalignment can optimize power production by redirecting wakes away from downstream turbines, thereby minimizing structural loads and net power losses [6], [7]. Various computational models and large eddy simulations have been used to quantify and maximize these potential power gains [7].

To further enhance wind farm performance, various methods have been proposed. These include a learning model predictive control (LMPC) algorithm, which produces up to 15% more power than conventional methods in offshore wind farms, and a data-driven stochastic model predictive control (SMPC) method that improves power production by 2.64% using Gaussian mixture model clustering for active yaw control [13]. High-fidelity simulation models such as PALM have also been implemented for power tracking, demonstrating better performance than greedy control [15]. Tools such as FLORIS have facilitated the development of data-driven multi-objective predictive control strategies based on evolutionary optimization [16]. Additionally, research has been conducted to maximize the power output of wind farms by determining the optimal yaw using a data-driven approach introduced as an alternative to FLORIS [17]. Furthermore, reinforcement learning has been extensively studied to maximize the power output of wind farms [18], [19], [20].

Despite these advances, wind farms, as complex systems, still face challenges in accurate modeling and control due to the vast amount of data and calculations involved. Model reduction methods are essential for achieving computational efficiency and real-time control [21], [22], [23], [24], [25], [26], [27], [28], [29], [30]. These methods reduce the complexity of models while retaining essential dynamics, making them suitable for practical applications. Significant strides have been made in this area. For instance, DMD with control (DMDc) has been developed to create precise input-output models for high-dimensional systems, effectively distinguishing between system dynamics and actuation effects [27]. Another study demonstrated that DMDc can generate reduced-order models for real-time control of high-dimensional systems such as thermal actuators [28]. Additionally, Koopman-based MPC with morphing surface techniques has shown that active flow control with a morphing flap can effectively regulate flow-induced vibrations and provide insights into environmental changes [29]. Research on distillation columns using MPC based on the DMD method revealed that DMD can construct accurate linearized models for predicting state variables, significantly improving control performance in nonlinear systems [30].

However, the application of model reduction techniques specifically for wind farm control remains limited, indicating a significant research gap that needs to be addressed to improve the efficiency and effectiveness of wind farm operations. To bridge this gap, this study introduces a data-driven approach using model predictive control (MPC) based on dynamic mode decomposition with input and output for reduced-order models (DMDior) to derive a reduced-order model (ROM) of a wind farm to enhance power production. In DMDc or DMDio, the system is first identified and then approximated with a ROM. In contrast, DMDior directly identifies the ROM, which is more computationally efficient and better suited for handling millions of nodes in flow fields. The study focuses on transforming comprehensive high-dimensional aerodynamic flow data within a wind farm into an accurate and manageable ROM. This model effectively represents the important dynamics of wind flow, including critical turbine interactions and the adaptive response of turbines to environmental changes. Using this ROM, we developed a detailed MPC framework to dynamically adjust the yaw angle of a wind turbine and maximize power output in response to constantly changing wind patterns. An important feature of our system is the incorporation of a carefully designed adaptive Kalman filter [31], [32], [33], [34] for accurate state estimation within the MPC framework. This estimation is critical to the efficient functioning of MPC, ensuring that operational decisions can be made based on the most up-to-date and accurate understanding of the state of the wind farm, significantly improving the reliability and efficiency of the control strategy. This approach provides a viable solution for improving the power production of
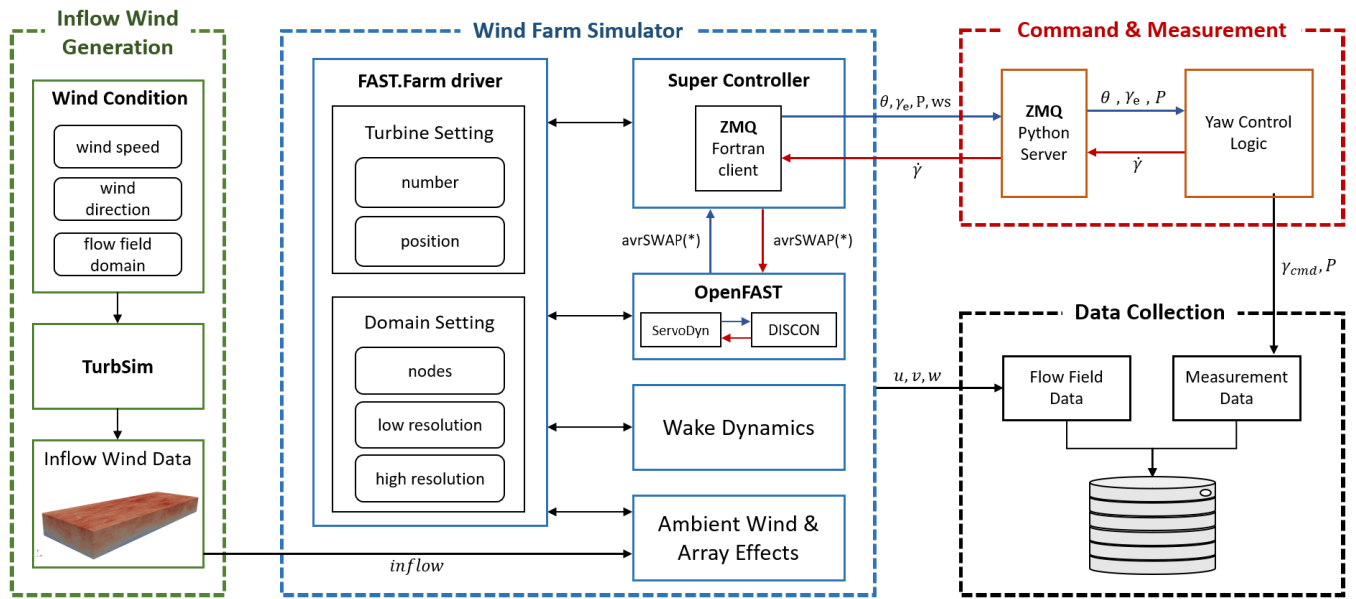
FIGURE 1. Overview of the data collection process.

wind farms, as demonstrated by results showing improved outcomes compared to traditional greedy control schemes. It also represents a significant advance in control strategies for wind energy systems and lays a solid foundation for continued research and development in this area.

This paper is organized as follows: Section II presents a methodology for generating a ROM suitable for wind farm control. Section III describes the design and integration of model predictive control based on these models by incorporating state estimation via Kalman filters. In Section IV, we present simulation results that show how effective our approach is compared to traditional greedy control methods. Finally, Section V concludes the paper with the main insights and implications of our findings.

II. REDUCED ORDER MODEL FOR WIND FARM CONTROL
A. SNAPSHOT DATA CONSTRUCTION
The development of a ROM to optimize yaw control in wind farms begins with the step of constructing snapshot data. This data captures specific instances of the wind farm's flow dynamics over time and comprises the velocity vectors of the wind farm's flow field. It was meticulously collected over a period of 1,000 seconds. The entire data collection process, which demonstrates our comprehensive methodology, is depicted in Figure 1.

To generate accurate inflow wind data, we employed TurbSim [35], developed by the National Renewable Energy Laboratory (NREL). This is known for its proficiency in simulating realistic atmospheric boundary layer conditions. This capability is vital for authentic simulations of individual wind turbines and entire wind farms. For our study, TurbSim was configured to simulate a flow field under specific conditions: a mean wind speed of $8 m/s$, a mean wind

direction of 0° (indicating wind coming from the west), and a turbulence intensity (TI) of 6%. Additionally, we employed the IEC Kaimal turbulence model, as defined in IEC 61400-3. Figure 2 shows the wind conditions according to the simulation time. This setup was strategically chosen to effectively demonstrate the impact of yaw control on our wind farm layout, taking into account factors such as prevailing wind directions and the geography of the wind farm.
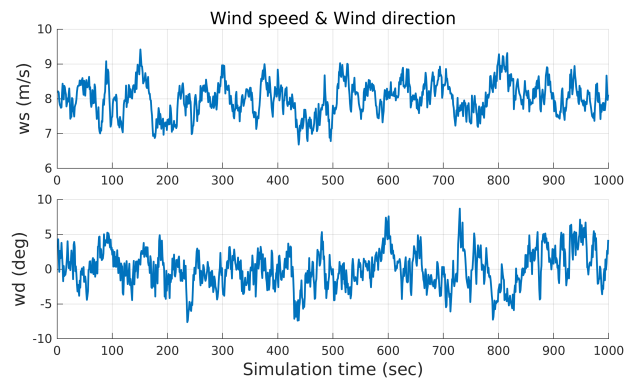

FIGURE 2. Wind speed and direction of the flow field generated by the Turbsim.

FAST.Farm [36] was chosen as our simulation tool because it provides a balanced approach for capturing the complex aerodynamic interactions within wind farms while ensuring computational efficiency. This medium-fidelity simulation tool incorporates components such as the FAST.Farm driver, super controller, openFAST [37], wake dynamics, and modules for ambient wind and array effects. These components are instrumental in accurately modeling the wind farm dynamics. The integration of ZeroMQ [38] enables

seamless and efficient communication between Fortran, used in FAST.Farm, and Python, utilized for the control logic. This integration allows for the data processing and control adjustments.

The upper right corner of Figure 1 illustrates the data exchange between FAST.Farm and the control logic. The measurements of FAST.Farm, which include the yaw angle θ, the yaw error γ_e, the electrical power P, and the wind speed of each turbine, send to the control logic. The yaw rate $\dot{\gamma}$ is the input into the super controller, which then controls the yaw angle of the turbine using OpenFAST within FAST.Farm. Meanwhile, both yaw offset γ and yaw error γ_e quantify the angle between the actual wind direction and the turbine's yaw orientation. Yaw offset references the wind direction, while yaw error is relative to the turbine's yaw position. These parameters, especially γ and P are important for identifying wind flow fields and for *posterior* state estimation via the Kalman filter.
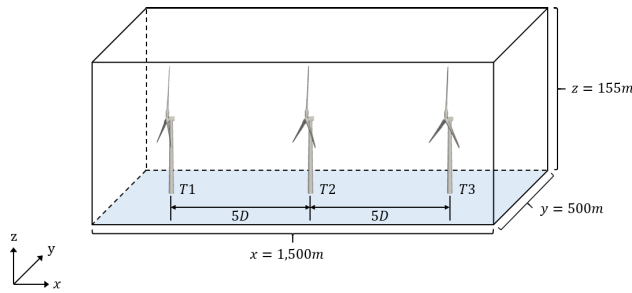

FIGURE 3. Turbine layout.

In this study, the wind farm layout was designed as a 1×3 turbine arrangement, with turbines positioned side by side at intervals of $5D$ (where D represents the turbine diameter, $126m$), as shown in Figure 3. The 1×3 turbine layout, though compact, was selected because it represents the smallest unit of a wind farm sufficient to observe the influence of wake interactions on power generation. This arrangement allows for a focused study of the impact of wake effects on turbine efficiency within the farm. The turbines employed in our simulation were modeled after the NREL 5MW reference turbine [39], widely recognized as a benchmark model in wind turbine research. This specific turbine model and layout were integrated into the FAST.Farm module, aiming to realistically represent the aerodynamic interactions within the farm.

We utilized FAST.Farm to collect a comprehensive dataset, including velocity components (u, v, w) and important turbine metrics such as yaw angle and power. This dataset was instrumental in developing a ROM through Dynamic Mode Decomposition with Input and Output for Reduced-order model (DMDior). This approach allowed us to create a model that accurately captures the operational dynamics of wind farms. The ROM derived from this extensive FAST.Farm data is essential for accurately modeling wind farm dynamics and enhancing their power output.

B. DIMENSIONALITY REDUCTION USING DMDIOR
1) DYNAMIC MODE DECOMPOSITION WITH INPUT AND OUTPUT FOR REDUCED-ORDER MODEL

In wind farm system analysis, dealing with complex, high-dimensional systems requires sophisticated modeling. Dynamic Mode Decomposition (DMD) [40], a technique that simplifies complex dynamics into more manageable low-dimensional representations, is effective but has limitations, notably its inability to factor in external inputs and outputs. Addressing this, our research introduces a refined model, DMDior, which builds on standard DMD by integrating both control inputs and system outputs. This significant enhancement facilitates a deeper understanding of turbine dynamics, particularly for yaw control in varying wind conditions, leading to improved operational efficiency and energy production in wind farms. By including input and output data in the DMD framework, DMDior offers a more efficient, comprehensive tool for analyzing and optimizing wind farm performance.

Let us consider the unknown discrete time system we aim to identify as follows:

$$\begin{aligned} x_{k+1} &= Ax_k + Bu_k \\ y_k &= Cx_k + Du_k \end{aligned} \quad (1)$$

where $x_k \in \mathbb{R}^n, u_k \in \mathbb{R}^p$, and $y_k \in \mathbb{R}^q$ are state, input and output vectors respectively. Matrices $A \in \mathbb{R}^{n \times n}, B \in \mathbb{R}^{n \times p}, C \in \mathbb{R}^{q \times n}$, and $D \in \mathbb{R}^{q \times p}$ are the state matrix constituting the state space representation. The dimensions p and q of the input and output are generally very small values compared to n, $(p, q \ll n)$. The DMDior algorithm can be divided into following steps:

1) Snapshot data collection and matrix representation:
   The snapshot data u_k and y_k of m state variables snapshot data x_k and $(m-1)$ inputs and outputs are collected and expressed in matrix form as in (2). where u_k is an arbitrary input and X' is a matrix that shifted X by time step.

$$\begin{aligned} X &= [x_1, x_2, \ldots, x_{m-1}] \in \mathbb{R}^{n \times (m-1)} \\ X' &= [x_2, x_3, \ldots, x_m] \quad \in \mathbb{R}^{n \times (m-1)} \\ I &= [u_1, u_2, \ldots, u_{m-1}] \in \mathbb{R}^{p \times (m-1)} \\ Y &= [y_1, y_2, \ldots, y_{m-1}] \quad \in \mathbb{R}^{q \times (m-1)} \end{aligned} \quad (2)$$

2) Calculate the singular value decomposition (SVD) of the matrix X and $\bar{\Omega}$:

$$X = U\Sigma V^T \approx U_r \Sigma_r V_r^T \quad (3)$$

where $U \in \mathbb{R}^{n \times n}, \Sigma \in \mathbb{R}^{n \times (m-1)}, V \in \mathbb{R}^{(m-1) \times (m-1)}, U_r \in \mathbb{R}^{n \times r}, \Sigma_r \in \mathbb{R}^{r \times r}$, and $V_r \in \mathbb{R}^{(m-1) \times r}$. The subscript r becomes a design variable as a truncation value to reduce the dimension of the system from n to r. The transformation matrix is determined using the snapshot proper orthogonal decomposition (POD) algorithm to determine the base coordinate axis that minimizes the prediction error.

Since the transformation matrix of the state variable is a transformation matrix, the left singular vector of the SVD of the matrix X must be used as the transformation matrix.

Then, the SVD of the matrix $\tilde{\Omega}$ is as follows:

$$\begin{bmatrix} X' \\ Y \end{bmatrix} = \begin{bmatrix} A & B \\ C & D \end{bmatrix} \begin{bmatrix} X \\ I \end{bmatrix}$$
$$= \begin{bmatrix} U_r \tilde{A} U_r^T & U_r \tilde{B} \\ \tilde{C} U_r^T & D \end{bmatrix} \begin{bmatrix} X \\ I \end{bmatrix} \quad (4)$$

This can be simplified to:

$$\begin{bmatrix} U_r^T X' \\ Y \end{bmatrix} = \begin{bmatrix} \tilde{A} & \tilde{B} \\ \tilde{C} & D \end{bmatrix} \begin{bmatrix} U_r^T X \\ I \end{bmatrix}$$
$$\approx \begin{bmatrix} \tilde{A} & \tilde{B} \\ \tilde{C} & D \end{bmatrix} \begin{bmatrix} \Sigma_r V_r^T \\ I \end{bmatrix}$$
$$Z = F \tilde{\Omega} \quad (5)$$

where $\tilde{\Omega} = \begin{bmatrix} \Sigma_r V_r^T \\ I \end{bmatrix} \in \mathbb{R}^{(r+p) \times (m-1)}$ is a matrix containing both a reduced product of singular value and right singular vector of state and input snapshot information, $Z = \begin{bmatrix} U_r^T X' \\ Y \end{bmatrix} \in \mathbb{R}^{(r+q) \times (m-1)}$ is a matrix containing a product of the reduced left singular vector of state and the shifted state matrix and output snapshot information, and $F = \begin{bmatrix} \tilde{A} & \tilde{B} \\ \tilde{C} & D \end{bmatrix} \in \mathbb{R}^{(r+q) \times (r+p)}$ is a matrix that DMDior wants to identify as a combination of the system's configuration matrix.

$$\tilde{\Omega} = \hat{U} \hat{\Sigma} \hat{V}^T \approx \hat{U}_s \hat{\Sigma}_s \hat{V}_s^T \quad (6)$$

where $\hat{U} \in \mathbb{R}^{(r+p) \times (r+p)}$, $\hat{\Sigma} \in \mathbb{R}^{(r+p) \times (m-1)}$, $\hat{V} \in \mathbb{R}^{(m-1) \times (m-1)}$, $\hat{U}_s \in \mathbb{R}^{(r+p) \times s}$, $\hat{\Sigma}_s \in \mathbb{R}^{s \times s}$, and $\hat{V}_s \in \mathbb{R}^{(m-1) \times s}$. The subscript s becomes a design variable as a truncated value.

3) Formulation of the Reduced Order Model:
The ROM is then expressed through new equations that represent the system dynamics in a lower-dimensional space:

$$\tilde{x}_{k+1} = \tilde{A} \tilde{x}_k + \tilde{B} u_k$$
$$y_k = \tilde{C} \tilde{x}_k + D u_k \quad (7)$$

where $x_k = U_r \tilde{x}_k$, and each matrix is as follows:

$$\begin{aligned} \tilde{A} &= U_r^T X' V_s \hat{\Sigma}_s^{-1} \hat{U}_1^T & \in \mathbb{R}^{r \times r} \\ \tilde{B} &= U_r^T X' V_s \hat{\Sigma}_s^{-1} \hat{U}_2^T & \in \mathbb{R}^{r \times p} \\ \tilde{C} &= Y V_s \hat{\Sigma}_s^{-1} \hat{U}_1^T & \in \mathbb{R}^{q \times r} \\ D &= Y V_s \hat{\Sigma}_s^{-1} \hat{U}_2^T & \in \mathbb{R}^{q \times p} \end{aligned} \quad (8)$$

where $\hat{U}_s^T = [\hat{U}_1^T \quad \hat{U}_2^T]$, $\hat{U}_1 \in \mathbb{R}^{r \times s}$, and $\hat{U}_2 \in \mathbb{R}^{p \times s}$.

4) Calculate eigenvalues, eigenvectors, and DMDior modes of reduction matrix $\tilde{A}$:
The eigenvalues and eigenvectors of matrix $\tilde{A}$ are as follows:

$$\tilde{A} w_i = \lambda_i w_i, \quad i = 1, 2, \ldots, r \quad (9)$$

The DMDior mode is calculated as follows:

$$\phi_i = X' \hat{V}_s \hat{\Sigma}_s^{-1} \hat{U}_1^T w_i \quad (10)$$

In this study, the DMDior algorithm is applied to the wind farm to construct a ROM of the wind farm.

2) APPLYING DMDIOR TO WIND FARM MODEL

In our research focusing on wind farm control using DMDior, we have identified key parameters that reflect the complex environmental and operational conditions typical of wind farms. Selecting these parameters was important to ensuring the accuracy and relevance of our ROM.

The foundation of our study is a dataset comprising 999 snapshots, collected over a simulation period of 1,000 seconds. Each snapshot contains 2,433,696 values, providing an extensive and detailed temporal representation of the wind farm's dynamics and capturing its operational complexity over time. As illustrated in Figure 3, We utilized FAST.Farm for the simulation, setting the field dimensions to $(x, y, z) = (1, 500, 500, 155)(m)$. The grid was designed with 251 points on the x-axis, 101 points on the y-axis, and 32 points on the z-axis, with intervals of 6 m, 5 m, and 5 m, respectively. This spatial configuration is well-suited to accurately capture the interactions within the wind farm, including the dynamics between individual turbines.

In our methodology, a pivotal step was the normalization of collected data for effective matrix representation in the DMDior process. This was essential given the high-dimensional and nonlinear characteristics of wind farm dynamics. Specifically, the state variable matrix $X \in \mathbb{R}^{2,433,696 \times 999}$ was normalized to ensure all data were in a dimensionless format. This normalization enabled uniform contributions from each variable across different datasets, enhancing the numerical stability and performance of the DMDior algorithm. Concurrently, data for the matrix $Y \in \mathbb{R}^{3 \times 999}$ was collected in MegaWatt (MW) units, and the input matrix $I \in \mathbb{R}^{3 \times 999}$ was collected in degrees (°). Combining a dimensionless representation for X and MW units for Y was important to maintaining the integrity and relevance of the information, ensuring accurate representation and analysis within our wind farm model.

DMDior in our study serves not only as a technique for dimensionality reduction but also as a method for preserving the unique dynamic characteristics of the original system. We conducted a detailed study to determine the truncation value, aiming to achieve a balanced representation of the complex and nonlinear characteristics of wind farm dynamics. Our goal was to identify a truncation value that satisfies both the observability and controllability of the dynamic behaviors captured by the model.

Through these experiments, we determined that the 36-dimensional model strikes an optimal balance between capturing the essential dynamics of the wind farm and maintaining computational efficiency. The 36-dimensional model was chosen because it adequately preserved the key dynamic interactions within the wind farm flow field

without introducing unnecessary computational complexity. Detailed comparisons showed that models with fewer dimensions failed to capture important dynamics, while models with more dimensions did not provide significant improvements but increased computational load. Therefore, the 36-dimensional model provides a reliable foundation for further analysis and the development of control strategies, effectively preserving the essential dynamics of the wind farm system.

The ROM we designed is suitable for applying model predictive control. This model will serve as a state-space model within the Model Predictive Control (MPC) algorithm.

C. VALIDATION OF THE REDUCED-ORDER MODEL

In this study, we validated the ROM created using DMDior. Our validation process aimed to assess the accuracy and reliability of the ROM by employing novel inputs not used during the model's construction phase. Figure 4 illustrates the input signals used for both the construction and subsequent validation of the model. We employed these signals because they provide distinct transitions that help in capturing the system's dynamic response. These signals allow us to observe the system's reaction to sudden changes, making it easier to model the wind farm's dynamics accurately. Inputs used to identify the model are represented by solid blue lines, while those used for validation are depicted as dashed red lines. This deliberate methodological choice ensures a comprehensive evaluation of the ROM's performance with new input signals.

For the specific case of the 1×3 turbine configuration, which involves turbines T1, T2, and T3 arranged from west to east, targeted strategies were implemented. These strategies included controlled adjustments to the yaw angles of all turbines in response to the wind direction variations, optimizing their aerodynamic efficiency. A pivotal step in our methodology was the deliberate introduction of a noise component into the input signals before applying the DMDior technique for ROM development. To this end, Gaussian noise e, characterized by $e \sim N(0, 0.1)$, was added to the inputs to more accurately simulate operational variabilities. The augmented input signal, incorporating this noise, is mathematically expressed as follows:

$$\tilde{u}(t) = u(t) + e \qquad (11)$$

where $\tilde{u}(t)$ denotes the noise-augmented input signal, $u(t)$ represents the original input signal, and e signifies the Gaussian noise. This procedural detail was important for demonstrating how operational noise impacts the ROM's effectiveness and reliability. Our findings show that incorporating noise not only tests the model's resilience but also significantly increases its robustness and real-world utility. The ability of the model to accommodate noise highlights a substantial improvement in its generalization capabilities, a vital aspect for dynamic systems like the wind turbine configurations explored in this study.

To validate the ROM, it was essential to compare the reconstructed flow fields from the ROM with the original
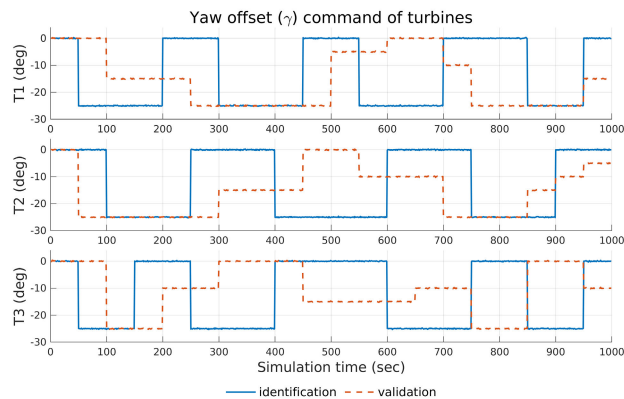

FIGURE 4. Input signal profiles for DMDior model identification and validation.

models derived from FAST.Farm simulations. By examining and quantifying the discrepancies between these flow fields, we were able to assess the ROM's fidelity. Given that the wind speed in front of the turbine rotor significantly affects power generation, our comparison specifically targeted the velocity components in this critical region. Particularly, at moments 200, 400, and 800 seconds, we focused on the Y-Z plane to provide a clear visual representation of the original flow fields, the reconstructed flow fields from the ROM, and the errors between them. As demonstrated in Figure 5, this comparison effectively illustrates that the ROM accurately captures the characteristics of the original model, thereby confirming its validity and the precision of its reconstruction capabilities.

Throughout the simulation period, we conducted a thorough analysis of errors related to the primary velocity components: u (aligned with the x-axis), v (along the y-axis), and w (along the z-axis), denoted as E_u, E_v, and E_w, respectively. To comprehensively assess the combined errors from these three dimensions, we introduced the total velocity error magnitude, E_U, which is defined as error of $U = \sqrt{u^2 + v^2 + w^2}$. This measure, depicted in Figure 6, illustrates the progression of errors for each velocity component throughout the simulation, measured in meters per second (m/s). Despite observing significant errors during transitions from impulse response to steady state in the model development phase, the average error remained around 1.18 m/s, underscoring the model's notable accuracy.

Additionally, Table 1 provides a closer look at the dynamics in front of the rotor, detailing the minimum, maximum, average, and standard deviation for each velocity component at this critical location across different turbines. The comprehensive data confirm the ROM's ability to accurately capture the essential dynamics of the flow field, maintaining errors within acceptable limits, especially for the velocity components at the forefront of the rotor. This combined analysis underscores the ROM's precision and effectiveness in modeling the behavior of the flow field, highlighting its value in simulations involving complex aerodynamic interactions.
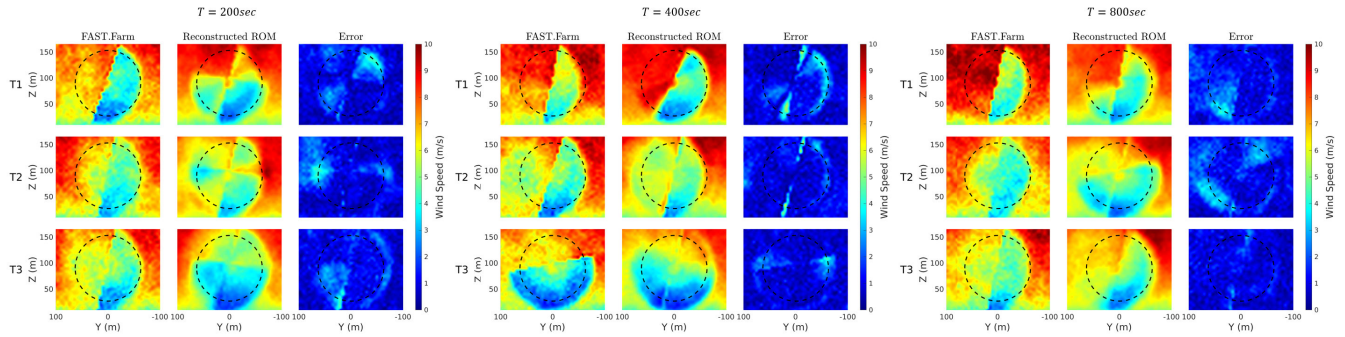
FIGURE 5. Comparison of FAST.Farm data and reconstruction data. The dashed circle indicates the diameter of a NREL 5MW turbine.
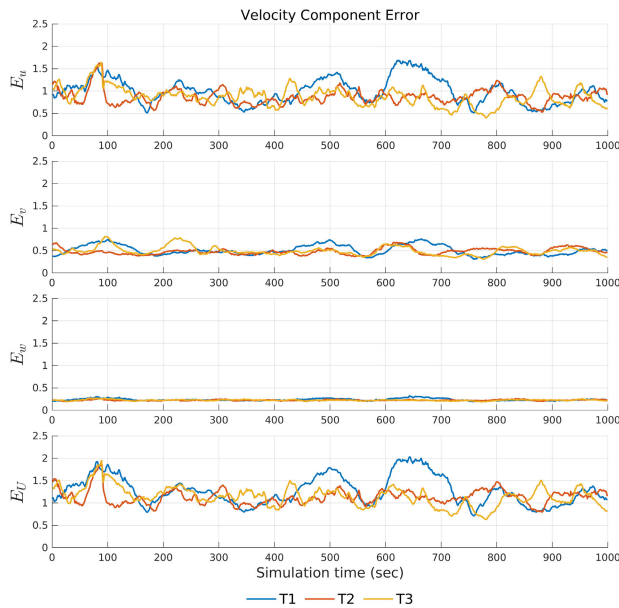

FIGURE 6. Simulation errors in velocity components u, v, w according to simulation time.

TABLE 1. Velocity component error according to simulation time.

Turbine	Component	Min	Max	Mean	Std
T_1	u	0.5090	1.6865	0.9936	0.2801
	v	0.3113	0.7624	0.5095	0.1096
	w	0.1931	0.3207	0.2377	0.0248
	U	0.7150	2.0286	1.2735	0.3196
T_2	u	0.5246	1.6250	0.8713	0.1637
	v	0.3655	0.6874	0.4826	0.0707
	w	0.1951	0.2632	0.2247	0.0123
	U	0.7951	1.8527	1.1345	0.1639
T_3	u	0.4005	1.6425	0.8754	0.2065
	v	0.3079	0.8150	0.4956	0.0963
	w	0.1866	0.2746	0.2253	0.0142
	U	0.6310	1.9514	1.1487	0.2155

This validation process, enhanced by comprehensive statistical and graphical analysis, confirms that the ROM effectively captures the wake dynamics of the wind farm system, maintaining an acceptable error margin, particularly for the velocity components at the front of the rotor. The

robustness and reliability of the model are thus firmly established, paving the way for the development of advanced and effective wind farm management strategies.

III. IMPLEMENTATION OF MODEL PREDICTIVE CONTROL WITH KALMAN FILTER

A. PROBLEM FORMULATION FOR MPC IN WIND FARM CONTROL

In this section, we outline the formulation of the MPC problem, aiming to maximize the power output of a wind farm. The primary objective of this approach is to determine the optimal yaw offsets and yaw rates for the wind turbines. This strategy is designed to not only maximize power production but also adhere to operational constraints, ensuring the wind farm's safety and efficiency.

As we narrow our focus from the overarching goal of maximizing power production within the wind farm to the detailed implementation of our control strategy, the necessity to adapt to the dynamic and intricate nature of wind farm environments becomes clear. The time-varying wind conditions and the complex interactions between turbines demand a control strategy that is not only adaptive but also meticulously precise. Given the intricate challenges presented by wind energy production, the incremental MPC method stands out as particularly proper for this context. This approach, by modulating the differences between consecutive control inputs, offers a refined mechanism to handle the operational complexities inherent in managing wind farms. The distinguishing strength of incremental MPC lies in its precision—allowing for the meticulous adjustment of control actions. This ensures that each change not only aligns with the operational capabilities of the turbine actuators but also provides a safeguard against the potential instabilities that sudden shifts might provoke. Through this method, we can achieve a balance of optimal performance and stability, tailoring our control strategies to the nuanced demands of wind power maximization.

To implement this method, it is essential to redefine the system's dynamics by integrating incremented control inputs into an existing state-space model. The former model can be

defined by (7).

$$\begin{bmatrix} \tilde{x}_{k+1} \\ x_{u_{k+1}} \end{bmatrix} = \begin{bmatrix} \tilde{A} & \tilde{B} \\ O_{p \times r} & I_{p \times p} \end{bmatrix} \begin{bmatrix} \tilde{x}_k \\ x_{u_k} \end{bmatrix} + \begin{bmatrix} \tilde{B} \\ I_{p \times p} \end{bmatrix} \Delta u_k$$

$$y_k = \begin{bmatrix} \tilde{C} & D \end{bmatrix} \begin{bmatrix} \tilde{x}_k \\ x_{u_k} \end{bmatrix} + D \Delta u_k \qquad (12)$$

where Δu_k, x_{u_k}, and $x_{u_{k+1}}$ is defined as following.

$$\Delta u_k = u_k - u_{k-1}$$
$$x_{u_k} = u_{k-1}$$
$$x_{u_{k+1}} = x_{u_k} + \Delta u_k \qquad (13)$$

In the final formulation of the state-space model for our control strategy, the augmented state vector x_a can be succinctly expressed as seen in (14), which comprises the system states and control input vector.

$$x_a = \begin{bmatrix} \tilde{x} \\ x_u \end{bmatrix} \qquad (14)$$

The subsequent state x_a is determined by following:

$$x_{a_{k+1}} = A' x_{a_k} + B' \Delta u_k$$
$$y_k = C' x_{a_k} + D \Delta u_k \qquad (15)$$

Equation (15) represents the state-space model utilized for incremental MPC in FAST.Farm. Here, Δu_k symbolizes the incremental control input, that is, the yaw rate, and y_k signifies the system's output, namely, the electrical power output of the wind turbine. This comprehensive state-space representation encapsulates the dynamics of our control system, laying the groundwork for the optimized regulation of the yaw rates within the operational constraints of the wind farm.

The objective function of the MPC is pivotal to its efficacy in maximizing the wind farm power output. It is formulated as follows:

$$\max_{u_{t:t+N-1}} J = y_{t+N}^T \mathbf{Q}_f y_{t+N}$$
$$+ \sum_{j=0}^{N-1} \left(y_{t+j}^T \mathbf{Q} y_{t+j} - \Delta u_{t+j}^T \mathbf{R} \Delta u_{t+j} \right) \qquad (16)$$

where y represents the power output from each turbine. The function spans a performance interval N, with j, the length of the horizon, set to 10. For the optimization process, the weighting factors $\mathbf{Q}_f$ and $\mathbf{Q}$ are utilized as identity matrix $I_{3 \times 3}$, and $\mathbf{R}$ is implemented as $0.1 * I_{3 \times 3}$, to finely tune the optimization. These specific settings are instrumental in adjusting the optimization process to achieve desired outcomes.

The operational constraints are a critical component of the MPC framework. These constraints involve limitations on the yaw offsets γ_i of the turbines, which are the essential in preventing mechanical stress and reducing aerodynamic interference between turbines, thereby preserving efficiency. Specifically, the yaw offsets for turbines T_1 and T_2 are constrained between $\gamma_{\min} = -25°$ and $\gamma_{\max} = 0°$.

In addition to these positional constraints, the rate of change of the yaw offsets, denoted as $\dot{\gamma}_{\min} = -0.3°/s$ and $\dot{\gamma}_{\max} = 0.3°/s$. These limits are imposed to avoid rapid yaw movements that could cause mechanical strain or reduce the aerodynamic performance of the turbines. This range optimizes their aerodynamic performance and avoids damaging loads. The turbine T_3, on the other hand, employs a greedy control strategy, maintaining a yaw offset of $0°$ because it operates downstream. This constraint allows for responsive yet controlled adjustments in each turbine's orientation, essential for maintaining structural integrity and operational stability. The formal constraints for yaw offsets are expressed as follows:

$$x_{a_{t+j+1}} = A' x_{a_{t+j}} + B' \Delta u_{t+j}, \quad j = 0, \dots, N-1 \qquad (17)$$
$$\gamma_{\min} \leq u_i \leq \gamma_{\max}, \quad i = 1, 2, 3$$
$$\dot{\gamma}_{\min} \leq \Delta u_i \leq \dot{\gamma}_{\max}, \quad i = 1, 2, 3 \qquad (18)$$

where u_i denotes the yaw offset of the i-th turbine that i is the number of the turbine, and j is the horizon length of the MPC. This constraint is instrumental for the MPC in making decisions that balance immediate power production objectives with the long-term condition and efficiency of the wind farm.

In terms of computational considerations, reducing the state-space model to 36 dimensions has significantly streamlined the computational process. The reduced matrices $\tilde{A} \in \mathbb{R}^{36 \times 36}$, $\tilde{B} \in \mathbb{R}^{36 \times 3}$, $\tilde{C} \in \mathbb{R}^{3 \times 36}$, and $D \in \mathbb{R}^{3 \times 3}$ enhance computational efficiency by reducing demands on storage and memory. Such efficiency is important for the applications and large-scale implementations, ensuring that the model remains both practical and responsive.

B. STATE ESTIMATION VIA KALMAN FILTERING

The design of the Kalman filter in our wind farm control system is tailored to effectively interpret the noisy and uncertain data characteristic of wind energy environments. This precision is important for achieving accurate state estimation, which directly influences the efficiency and reliability of the MPC. Therefore, we introduced an Adaptive Kalman Filter (AKF), which improves the ability to adjust its parameters, enhancing the system's responsiveness to changing environmental conditions. This characteristics of the AKF enabled us to evaluate the practicality of our wind farm control system more effectively. By adapting to the dynamics of the wind farm environment, the AKF ensured more reliable and robust state estimations.

1) IMPLEMENTATION OF ADAPTIVE KALMAN FILTER

Our AKF design involves calibrating its parameters to align with the dynamics of the wind farm as represented by the ROM. The variable $\tilde{x}_k$ represents a state variable that has been dimensionally reduced to r dimensions from an original n dimensional wind flow field. The variables u_k and z_k are the yaw offset and the power of each turbine. The random noise variables $w_k \in \mathbb{R}^r$ and $v_k \in \mathbb{R}^q$ respectively represent

the process noise and the measurement noise. The state-space representation and measurement equation are formulated as follows:

$$\tilde{x}_{k+1} = \tilde{A}\tilde{x}_k + \tilde{B}u_k + w_k$$
$$z_k = \tilde{C}\tilde{x}_k + Du_k + v_k \quad (19)$$

where the subscript k is the time variable, which indicates the time step. the process noise w_k and the measurement noise v_k are assumed to be Gaussian distributed white noise as follows:

$$\mathbb{E}[w_k] = 0, \ \mathbb{E}[v_k] = 0, \ \mathbb{E}[w_i v_j^T] = 0, \ \forall i = j \in \mathbb{N} \quad (20)$$
$$\mathbb{E}[w_i w_j^T] = Q_k, \quad \mathbb{E}[v_i v_j^T] = R_k, \quad \forall i = j \in \mathbb{N} \quad (21)$$

where covariance matrices Q_k for the process noise and R_k for the measurement noise at step k as in (21).

The AKF algorithm is an iterative process of correction-prediction steps. In the correction step, the prior variables are employed to refine the posterior variables, whereas in the prediction step, posterior variables are utilized to update the prior variables. Equations (22) to (25) formalize the Kalman filter algorithm.

Step 1 - Initialization:

$$\hat{\tilde{x}}_{-1|-1} = \mathbb{E}[\tilde{x}_{-1}]$$
$$P_{-1|-1} = \mathbb{E}[(\tilde{x}_{-1} - \hat{\tilde{x}}_{-1|-1})(\tilde{x}_{-1} - \hat{\tilde{x}}_{-1|-1})^T] \quad (22)$$

where the subscript "$k|k$" denotes *a posteriori* state. Specifically, $\hat{\tilde{x}}_{-1|-1}$ represents the initial *posteriori* state estimate, and $P_{-1|-1}$ represents the initial *posteriori* covariance matrix.

Step 2 - Prediction:

$$\hat{\tilde{x}}_{k|k-1} = \tilde{A}\hat{\tilde{x}}_{k-1|k-1} + \tilde{B}u_{k-1}$$
$$P_{k|k-1} = \tilde{A}P_{k-1|k-1}\tilde{A}^T + Q_{k-1} \quad (23)$$

where the subscript "$k|k-1$" denotes *a priori* state. The *priori* state estimate $\hat{\tilde{x}}_{k|k-1}$ is predicted through the dynamic relationship between the *posteriori* state estimate and control inputs. The *priori* covariance matrix $P_{k|k-1}$ is updated based on the *posteriori* covariance matrix and the process noise covariance Q_{k-1}.

Step 3 - Correction:

$$\hat{z}_{k|k-1} = \tilde{C}\hat{\tilde{x}}_{k|k-1} + Du_k$$
$$S_k = \tilde{C}P_{k|k-1}\tilde{C}^T + R_k$$
$$K_k = P_{k|k-1}\tilde{C}^T S_k^{-1} \quad (24)$$
$$\hat{\tilde{x}}_{k|k} = \hat{\tilde{x}}_{k|k-1} + K_k(z_k - \hat{z}_{k|k-1})$$
$$P_{k|k} = P_{k|k-1} - K_k S_k K_k^T \quad (25)$$

where $\hat{z}_{k|k-1}$ is the *priori* measurement estimate predicted from the *priori* state estimate. S_k is the innovation covariance and K_k is the kalman gain as in (24).

In (25), $\hat{\tilde{x}}_{k|k}$ represents the *posteriori* state estimate, which subsequently serves as an input to the MPC to determine the optimal control inputs for FAST.Farm. Additionally, $P_{k|k}$ indicates the *posteriori* covariance matrix.

Kalman filter design variables like Q_{k-1}, R_k, and P_0 are set using system knowledge and empirical methods. Yet, physical relevance can be lost when reducing matrix A dimensions with DMDior, which may render system knowledge impractical and trial-and-error costly in finding correct covariances. To address these challenges, we designed an AKF by drawing on the methodologies and insights presented in the studies [31], [32], [33], [34].

At each time step, the AKF updates the noise covariances Q_{k-1} and R_k using 'innovation' and 'residual', respectively. the innovation d_k is the difference between the measurement z_k and the *priori* measurement estimate $\hat{z}_{k|k-1}$ as in (26). In contrast, the residual ε_k is the difference between the measurement z_k and the *posteriori* measurement estimate $\hat{z}_{k|k}$ estimated from the *posteriori* state estimate as in (29).

The formulas that are represented in (27) and (30), which offer an innovation or residual-based approach for adaptive estimation, have been proven by [32]. Building on this foundation, [31] advanced the approach by proposing a delayed updating method that utilizes a forgetting factor about the noise covariances. We adopted this delayed updating method, and it is incorporated into (28) and (31).

- Update the Q_{k-1} with innovation:

$$\hat{z}_{k|k-1} = \tilde{C}\hat{\tilde{x}}_{k|k-1} + Du_k$$
$$d_k = z_k - \hat{z}_{k|k-1} \quad (26)$$
$$w_{k-1} = \tilde{x}_k - (\tilde{A}\tilde{x}_{k-1} + \tilde{B}u_{k-1})$$
$$\hat{w}_{k-1} = \hat{\tilde{x}}_{k|k} - \hat{\tilde{x}}_{k|k-1}$$
$$= K_k(z_k - \hat{z}_{k|k-1}) = K_k d_k \quad (27)$$
$$\hat{Q}_{k-1} = \mathbb{E}[\hat{w}_{k-1}\hat{w}_{k-1}^T]$$
$$= \mathbb{E}[K_k(d_k d_k^T)K_k^T]$$
$$= K_k \mathbb{E}[d_k d_k^T]K_k^T$$
$$Q_k = \alpha Q_{k-1} + (1-\alpha)\hat{Q}_{k-1} \quad (28)$$

- Update the R_k with residual:

$$\hat{z}_{k|k} = \tilde{C}\hat{\tilde{x}}_{k|k} + Du_k$$
$$\varepsilon_k = z_k - \hat{z}_{k|k} \quad (29)$$
$$\hat{S}_k = \mathbb{E}[\varepsilon_k \varepsilon_k^T]$$
$$= \mathbb{E}[v_k v_k^T] - \tilde{C}P_{k|k}\tilde{C}^T$$
$$\hat{R}_k = \mathbb{E}[\varepsilon_k \varepsilon_k^T] + \tilde{C}P_{k|k}\tilde{C}^T \quad (30)$$
$$R_{k+1} = \alpha R_k + (1-\alpha)\mathbb{E}[\varepsilon_k \varepsilon_k^T] + \tilde{C}P_{k|k}\tilde{C}^T \quad (31)$$

where α is a forgetting factor [31], ($0 < \alpha < 1$), serving as an alternative to the moving window approach in the expectation of errors in [33] and [34]. This factor modulates update speed by equilibrating previous and emerging covariance values. Subsequent to the prediction phase, process noise covariance Q_{k-1} is refined employing (28). Post-correction, measurement noise covariance R_k undergoes updating via (31), preparing noise covariances for subsequent steps.

Updates to noise covariances commence from the time step at $k = 1$, excluding the initial time step at $k = 0$. Specifically, R_1 is set to R_0 when applying (31) at $k = 1$ for R_k.

2) VALIDATION OF KALMAN FILTER IN WIND FARM

This research on wind farm control systems places significant emphasis on the integration and validation of an AKF in conjunction with FAST.Farm, a medium-fidelity wind farm simulator. The next section will elaborate on the integration aspect, while this section focuses on the validation of the AKF.

To validate the AKF's effectiveness within a wind farm setting, we conducted a comprehensive simulation spanning 1,000 seconds using FAST.Farm. Post-simulation, the AKF's design was ascertained using actual measurements z_k against the predicted measurements $\hat{z}_{k|k-1}$. Figure 7 illustrates graphs comparing the actual power measured in FAST.Farm to the power predicted by the AKF over the same duration. The innovation, the difference between measured and predicted power, confirms its containment within the standard deviation range predicted by the AKF. The outcomes indicate that the AKF effectively predicted the turbines' power output.
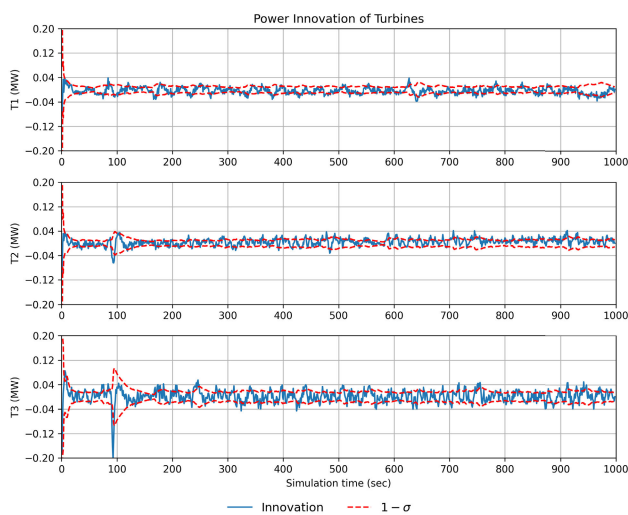

FIGURE 7. Power innovation and standard deviation for each turbine.

The level of accuracy achieved by the AKF not only validates its robustness but also emphasizes its essential role in optimizing operational efficiency and control within wind farm systems. Accurate state estimation, as facilitated by the AKF, is indispensable for the effective deployment of MPC strategies. These strategies rely heavily on precise and current data to optimize wind farm performance. The AKF's exemplary performance in this simulation strongly supports its practical implementation for managing and enhancing wind energy resources.

C. INTEGRATED MPC FRAMEWORK

The integration of MPC with an AKF represents a advancement in wind farm control systems, substantially enhancing both operational efficiency and power output. As shown in Figure 8, this synergistic framework combines the predictive capabilities of MPC with the precision of the AKF. This integration enables the optimal adjustment of turbine yaw angles, significantly improving overall wind farm performance.

This integrated approach focuses on accurately determining yaw angles for each turbine, a important factor in maximizing farm power output. The MPC, leveraging precise state predictions from the AKF, dynamically calculates the yaw rate for each turbine to achieve the optimal yaw angles. These calculations consider various parameters, including wind speed, direction, and interactions between turbines, to ensure optimal power output under diverse operational conditions.

In this setup, the AKF plays an essential role in continuously updating the wind farm's state estimates, utilizing measurement data from FAST.Farm. This data accurately reflects the wind farm's true operational conditions and is processed through the ROM. Consequently, the Kalman filter provides the MPC, detailed insights into the farm's status, including critical aspects such as wind patterns and turbine metrics. This capability is pivotal for the MPC to make accurate predictions of future states and to adjust yaw angles subsequently to maximize power output. The integrated system is designed not only to enhance immediate power output but also to improve the long-term efficiency and sustainability of the wind farm.

IV. RESULTS AND ANALYSIS
A. SIMULATION RESULTS

This section presents the results of our simulations, aimed at evaluating the performance of the proposed approach. The wind conditions used in these simulations are shown in Figure 2. The results provide valuable insights into our approach's effectiveness.

The simulation results demonstrate the efficacy of the proposed approach in maximizing the power output of a wind farm within the given constraints. The simulation was conducted over 1,000 seconds to provide a sufficient timeframe for observing the impact of wake effects and the performance of control strategies, considering it takes approximately 200 seconds for the wind to propagation from Turbine T1 to T3. This duration allows for a comprehensive evaluation of the MPC framework's efficiency, considered appropriate for assessing its performance relative to greedy control.

Figure 9 displays the outcomes for the optimal yaw offset for each turbine alongside the turbine's yaw offset. The turbine's yaw offset is indicated by the blue solid line, while the red solid line represents the optimal yaw offset determined by the MPC. T1 and T2 effectively apply the turbine's yaw offset along the optimal yaw offset value, while T3 is adjusted to produce maximum power through greedy control.

Figure 10 illustrates a comparative power output graph over a period of 1,000 seconds. The blue dotted line in
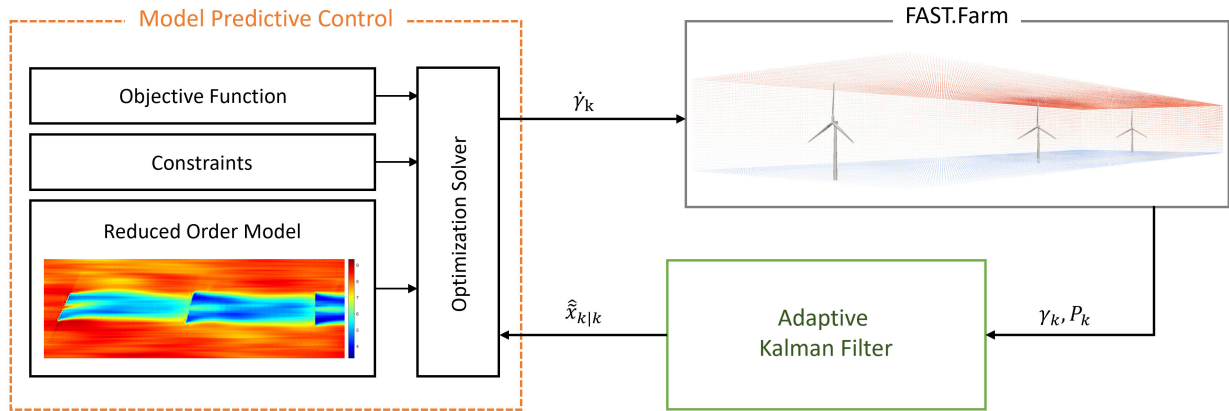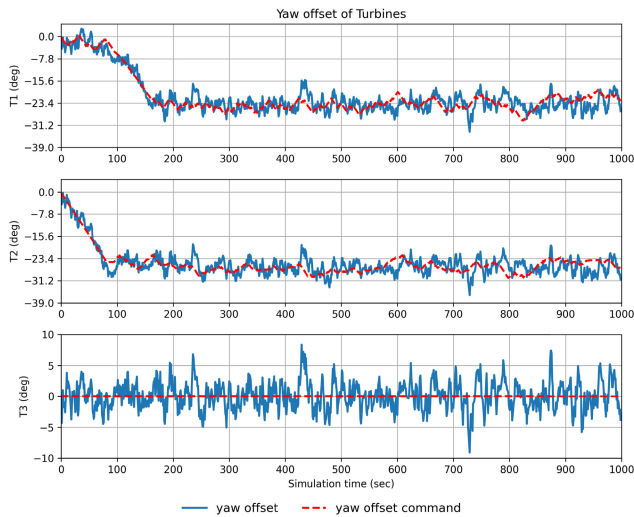
FIGURE 8. MPC framework.

FIGURE 9. Optimal yaw offset for each turbine.

FIGURE 10. Power for each turbine and farm.

the graph represents the power generated under greedy control, whereas the red solid line indicates the power output for the optimal yaw as calculated from the MPC model. Greedy control initially produces more power for Turbine T1, positioned at the front. However, for Turbines T2 and T3, MPC outperforms greedy control in terms of power generation. Up until about 250 seconds, greedy control performs better due to the wake effects in the simulation not yet significantly impacting the other turbines. This is the primary reason why greedy control initially produces more power. However, after this period, it becomes evident that controlling the yaw angles using the MPC framework results in greater power production than what is achieved with greedy control.

To evaluate the performance of MPC over a 1,000 second span, we introduced a metric called the power growth rate (PGR). This metric quantitatively demonstrates how much MPC surpasses greedy control in power generation. Additionally, for a clearer comparison another algorithm,
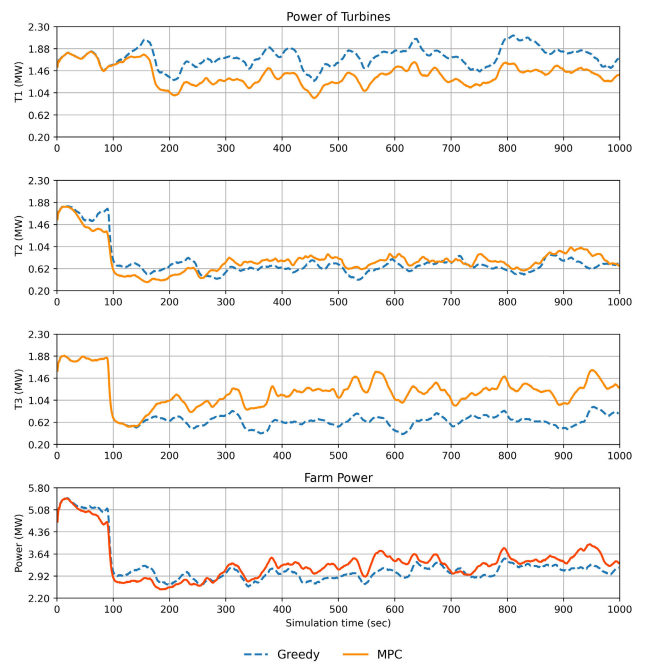
YDNN [17], which also output the yaw offset, were included in the comparison. The PGR calculation formulas are as follows:

$$PGR_{MPC}(\%) = \frac{P_{MPC} - P_{Greedy}}{P_{Greedy}} * 100. \quad (32)$$

$$PGR_{YDNN}(\%) = \frac{P_{YDNN} - P_{Greedy}}{P_{Greedy}} * 100. \quad (33)$$

YDNN include the first-order actuator model as shown in (34), which is given by:

$$\dot{\gamma} = (\gamma_{cmd} + \gamma_e)/\tau \quad (34)$$

This allows for a clearer comparison of the performance of MPC and YDNN. Figure 11 displays the cumulative

PGR, allowing a visual comparison of the cumulative power production by greedy control, MPC, and YDNN control methods. Initially, the greedy control produces more power than the other methods, but after 494 seconds, the MPC cumulatively generates more power than greedy control.
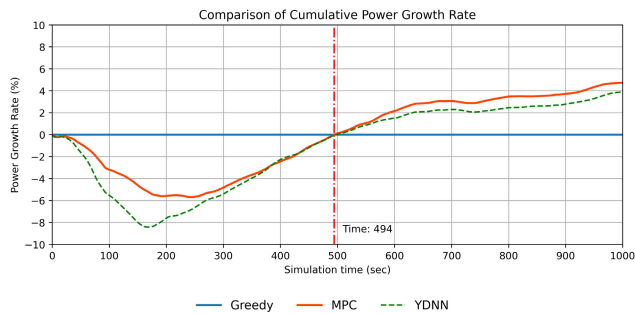

FIGURE 11. Comparison of cumulative PGR.

The proposed MPC in this study allows for finer adjustments, which results in faster recovery from wake effects compared to the another algorithm. This improved precision in controlling the yaw rate enables MPC to optimize power generation more effectively, demonstrating its superiority in adapting to dynamic conditions and maximizing overall efficiency.

Table 2 presents both the cumulative power generated by greedy control, MPC, and YDNN control, along with the calculated PGR, over a $1000sec$ simulation period. The results reveal that, the incremental MPC produced approximately $0.1522GW$ more energy than the greedy control method. This equates to an increase of about 4.72% in farm power output. This significant enhancement in power output underscores the efficacy of the incremental MPC approach, particularly in its ability to optimize the power output of the wind farm.

TABLE 2. Power comparison between greedy and MPC.

	Greedy	MPC	YDNN [17]
Cumulative power (GW)	3.2215	3.3737	3.3462
PGR (%)	0.0	4.7245	3.8708

B. DISCUSSION OF THE FINDINGS AND IMPLICATIONS

The analysis of the PGR demonstrates a significant improvement in power output resulting from the application of the MPC framework compared to greedy control in wind farm operations. This comparison highlights the direct advantages of implementing MPC and provides clear evidence of its superior performance over greedy control, showcasing the efficacy of MPC in enhancing the efficiency of wind farm power generation.

Greedy control requires each turbine to independently maximize its power output. This method necessitates separate wind speed and direction measurements for each turbine, leading to less efficient power production due to individual control and wake effects. In contrast, the MPC framework optimizes the entire farm's turbine alignment and operation collectively using upstream wind information. This strategy streamlines the control process by minimizing the need for individual turbine data and boosts farm efficiency through a coordinated approach that acknowledges turbine interdependencies.

A crucial component of our MPC framework is the integration of the AKF. The AKF provides accurate state estimation by correcting model predictions with real-time data. This integration is essential for dealing with uncertainties and noise in measurement data, thus enhancing the reliability and precision of the control strategy. By ensuring that the MPC framework has access to accurate and up-to-date information, the AKF significantly improves the ability of the MPC to adapt to changing wind conditions, resulting in better overall performance and stability.

The outcomes of this study pave the way for further investigations into the scalability of the MPC framework, especially under fluctuating wind conditions and intricate wind farm configurations. These findings imply the practical applicability of MPC in real-world scenarios. Moreover, the results represent the potential of MPC to augment the operational efficiency of wind farms, particularly in scenarios afflicted by wake effects. While the current study applies this approach to a 1×3 turbine layout, the efficacy of the MPC framework is expected to be applicable across a broader spectrum of conditions.

In summary, the key contributions of our MPC framework in this study are:

- *Dynamic optimization:* Enables continuous optimization of control parameters, ensuring turbines operate at optimal settings to maximize power output.
- *Simplified control via ROMs:* Utilizes reduced-order models to simplify complex aerodynamic interactions, allowing for rapid and precise control decisions.
- *Adaptability:* Adapts to changing wind patterns, making proactive adjustments based on time-varying data and forecasts.
- *Accurate state estimation with AKF:* Integrates the Adaptive Kalman Filter to improve control strategy reliability and precision, crucial for real-time adjustments and managing uncertainties.
- *Incremental control for fine-tuning yaw rates:* Employs an incremental approach to MPC, enabling fine adjustments to yaw rates, which further maximizes power production and reduces wake effects.

These features collectively demonstrate the potential of our MPC framework to significantly improve the performance and efficiency of wind farm operations under a variety of scenarios, highlighting its robustness and real-world applicability.

V. CONCLUSION

In this study, we successfully developed a ROM to maximize the power output of a wind farm using MPC. Initially,

a 36-dimensional ROM was designed via DMDior using snapshot data collected from FAST.Farm. This process was crucial for identifying and extracting the dynamic characteristics of the wind farm flow field. The ROM effectively captured the wake model, and its performance was validated through model reconstruction.

The developed ROM was integrated into the MPC framework to solve the optimization problem of maximizing wind farm power output. This approach facilitated the generation of the optimal yaw angle under time-varying wind conditions and was further enhanced by incorporating an adaptive Kalman filter for more realistic operational scenarios. The study results showed that the power output of the wind farm under this MPC approach was approximately 4.72% higher compared to the traditional greedy control scheme, demonstrating the effectiveness of our proposed method.

This study makes several key contributions to the field. We successfully developed a ROM that accurately captures the dynamic characteristics of wind farm flow fields, which is essential for effective control and optimization. By integrating this model with an MPC framework, we optimized turbine's yaw angles, resulting in significant improvements in power output. Furthermore, the inclusion of an AKF enhanced the realism and applicability of the MPC approach in operational scenarios by providing accurate state estimation. The simulation validation demonstrated a 4.72% increase in power output compared to traditional control methods, underscoring the practical effectiveness of our approach.

However, the limitations of the current study include the use of a linear model based on singular wind speed and direction. Future research will address these constraints by expanding beyond linear assumptions to incorporate more complex and variable wind conditions. This will enhance the MPC framework's applicability, enabling a more dynamic and flexible control system capable of adapting to wind complexities, thereby further improving the efficiency and reliability of wind farm operations.

In conclusion, this study provides a promising path to significantly advance the control and optimization techniques of wind farm operations, improving power generation and operational efficiency. Future work should aim to extend this study to include a wider range of wind farm configurations, evaluate its performance in real-world applications, and explore additional optimization techniques for further improvement. By addressing these areas, the practical impact and applicability of the proposed MPC framework can be significantly enhanced.

REFERENCES

[1] F. González-Longatt, P. Wall, and V. Terzija, "Wake effect in wind farm performance: Steady-state and dynamic behavior," *Renew. Energy*, vol. 39, no. 1, pp. 329–338, Mar. 2012. [Online]. Available: https://www.sciencedirect.com/science/article/pii/S0960148111005155

[2] M. F. Howland, S. K. Lele, and J. O. Dabiri, "Wind farm power optimization through wake steering," *Proc. Nat. Acad. Sci. USA*, vol. 116, no. 29, pp. 14495–14500, Jul. 2019, doi: 10.1073/pnas.1903680116.

[3] N. G. Nygaard and S. D. Hansen, "Wake effects between two neighbouring wind farms," *J. Phys., Conf.*, vol. 753, Sep. 2016, Art. no. 032020, doi: 10.1088/1742-6596/753/3/032020.

[4] T. K. Laursen, S. Sivabalan, A. B. Borchersen, and J. A. Larsen, "Wake-effect minimising optimal control of wind farms, with load reduction," *IFAC Proc. Volumes*, vol. 47, no. 3, pp. 6770–6775, 2014. [Online]. Available: https://www.sciencedirect.com/science/article/pii/S1474667016426765

[5] M. Kim, H. Lim, and S. Park, "Comparative analysis of wind farm simulators for wind farm control," *Energies*, vol. 16, no. 9, p. 3676, Apr. 2023. [Online]. Available: https://www.mdpi.com/1996-1073/16/9/3676

[6] M. T. van Dijk, J.-W. van Wingerden, T. Ashuri, Y. Li, and M. A. Rotea, "Yaw-misalignment and its impact on wind turbine loads and wind farm power output," *J. Phys., Conf.*, vol. 753, Sep. 2016, Art. no. 062013, doi: 10.1088/1742-6596/753/6/062013.

[7] C. L. Archer and A. Vasel-Be-Hagh, "Wake steering via yaw control in multi-turbine wind farms: Recommendations based on large-eddy simulation," *Sustain. Energy Technol. Assessments*, vol. 33, pp. 34–43, Jun. 2019. [Online]. Available: https://www.sciencedirect.com/science/article/pii/S2213138818306544

[8] X. Yu, Y. Liu, T. Chen, H. Meng, and L. Li, "Study on the yaw-based wake steering control considering dynamic flow characteristics for wind farm power improvement," *J. Phys., Conf.*, vol. 2505, no. 1, May 2023, Art. no. 012010, doi: 10.1088/1742-6596/2505/1/012010.

[9] U. Ciri, M. A. Rotea, and S. Leonardi, "Effect of the turbine scale on yaw control," *Wind Energy*, vol. 21, no. 12, pp. 1395–1405, Dec. 2018, doi: 10.1002/we.2262.

[10] P. M. O. Gebraad, F. W. Teeuwisse, J. W. van Wingerden, P. A. Fleming, S. D. Ruben, J. R. Marden, and L. Y. Pao, "Wind plant power optimization through yaw control using a parametric model for wake effects—A CFD simulation study," *Wind Energy*, vol. 19, no. 1, pp. 95–114, Jan. 2016, doi: 10.1002/we.1822.

[11] J. Meyers, C. Bottasso, K. Dykes, P. Fleming, P. Gebraad, G. Giebel, T. Göçmen, and J.-W. van Wingerden, "Wind farm flow control: Prospects and challenges," *Wind Energy Sci.*, vol. 7, no. 6, pp. 2271–2306, Nov. 2022. [Online]. Available: https://wes.copernicus.org/articles/7/2271/2022/

[12] J. Ebegbulem and M. Guay, "Power maximization of wind farms using discrete-time distributed extremum seeking control," *IFAC-PapersOnLine*, vol. 51, no. 18, pp. 339–344, 2018. [Online]. Available: https://www.sciencedirect.com/science/article/pii/S2405896318320056

[13] X. Yin and X. Zhao, "Data driven learning model predictive control of offshore wind farms," *Int. J. Electr. Power Energy Syst.*, vol. 127, May 2021, Art. no. 106639. [Online]. Available: https://www.sciencedirect.com/science/article/pii/S0142061520341843

[14] Y. Wang, S. Wei, W. Yang, and Y. Chai, "Robust active yaw control for offshore wind farms using stochastic predictive control based on online adaptive scenario generation," *Ocean Eng.*, vol. 286, Oct. 2023, Art. no. 115578. [Online]. Available: https://www.sciencedirect.com/science/article/pii/S0029801823019625

[15] S. Boersma, V. Rostampour, B. D. J.-W. van Wingerden, and T. Keviczky, "A model predictive wind farm controller with linear parameter-varying models," *IFAC-PapersOnLine*, vol. 51, no. 20, pp. 241–246, 2018. [Online]. Available: https://www.sciencedirect.com/science/article/pii/S2405896318326740

[16] X. Yin, W. Zhang, Z. Jiang, and L. Pan, "Data-driven multi-objective predictive control of offshore wind farm based on evolutionary optimization," *Renew. Energy*, vol. 160, pp. 974–986, Nov. 2020. [Online]. Available: https://www.sciencedirect.com/science/article/pii/S0960148120307138

[17] M. Kim and S. Park, "Data-driven approach for wind farm control: Toward an alternative to FLORIS," *IEEE Access*, vol. 12, pp. 13327–13339, 2024. [Online]. Available: https://ieeexplore.ieee.org/document/10410842

[18] H. Dong, J. Xie, and X. Zhao, "Wind farm control technologies: From classical control to reinforcement learning," *Prog. Energy*, vol. 4, no. 3, Jun. 2022, Art. no. 032006, doi: 10.1088/2516-1083/ac6cc1.

[19] P. Stanfel, K. Johnson, C. J. Bay, and J. King, "A distributed reinforcement learning yaw control approach for wind farm energy capture maximization," in *Proc. Amer. Control Conf. (ACC)*, Jul. 2020, pp. 4065–4070.

[20] Z. Deng, C. Xu, X. Han, Z. Cheng, and F. Xue, "Decentralized yaw optimization for maximizing wind farm production based on deep reinforcement learning," *Energy Convers. Manag.*, vol. 286, Jun. 2023, Art. no. 117031. [Online]. Available: https://www.sciencedirect.com/science/article/pii/S0196890423003771

[21] N. Cassamo and J.-W. van Wingerden, "Model predictive control for wake redirection in wind farms: A Koopman dynamic mode decomposition approach," in *Proc. Amer. Control Conf. (ACC)*, May 2021, pp. 1776–1782.

[22] B. Sharan, A. Dittmer, and H. Werner, "Real-time model predictive control for wind farms: A Koopman dynamic mode decomposition approach," in *Proc. Eur. Control Conf. (ECC)*, Jul. 2022, pp. 1006–1011.

[23] S. J. Andersen and J. P. Murcia Leon, "Predictive and stochastic reduced-order modeling of wind turbine wake dynamics," *Wind Energy Sci.*, vol. 7, no. 5, pp. 2117–2133, Oct. 2022. [Online]. Available: https://wes.copernicus.org/articles/7/2117/2022/

[24] E. Smilden, J.-T. H. Horn, A. J. Sørensen, and J. Amdahl, "Reduced order model for control applications in offshore wind turbines," *IFAC-PapersOnLine*, vol. 49, no. 23, pp. 386–393, 2016. [Online]. Available: https://www.sciencedirect.com/science/article/pii/S2405896316320237

[25] G. V. Iungo, C. Santoni-Ortiz, M. Abkar, F. Porté-Agel, M. A. Rotea, and S. Leonardi, "Data-driven reduced order model for prediction of wind turbine wakes," *J. Phys., Conf.*, vol. 625, Jun. 2015, Art. no. 012009, doi: 10.1088/1742-6596/625/1/012009.

[26] N. Cassamo and J.-W. van Wingerden, "On the potential of reduced order models for wind farm control: A Koopman dynamic mode decomposition approach," *Energies*, vol. 13, no. 24, p. 6513, Dec. 2020. [Online]. Available: https://www.mdpi.com/1996-1073/13/24/6513

[27] J. L. Proctor, S. L. Brunton, and J. N. Kutz, "Dynamic mode decomposition with control," *SIAM J. Appl. Dyn. Syst.*, vol. 15, no. 1, pp. 142–161, Jan. 2016, doi: 10.1137/15m1013857.

[28] D. Wolfram and T. Meurer, "DMD-based model predictive control for a coupled PDE-ODE system," *IFAC-PapersOnLine*, vol. 56, no. 2, pp. 4258–4263, 2023. [Online]. Available: https://www.sciencedirect.com/science/article/pii/S2405896323021985

[29] T.-K. Wang and K. Shoele, "Koopman-based model predictive control with morphing surface: Regulating the flutter response of a foil with an active flap," *Phys. Rev. Fluids*, vol. 9, no. 1, Jan. 2024, Art. no. 014702, doi: 10.1103/PhysRevFluids.9.014702.

[30] X. Qian, Q. Dang, S. Jia, Y. Yuan, K. Huang, H. Chen, and L. Zhang, "Operation of distillation columns using model predictive control based on dynamic mode decomposition method," *Ind. Eng. Chem. Res.*, vol. 62, no. 50, pp. 21721–21739, Dec. 2023, doi: 10.1021/acs.iecr.3c03275.

[31] S. Akhlaghi, N. Zhou, and Z. Huang, "Adaptive adjustment of noise covariance in Kalman filter for dynamic state estimation," in *Proc. IEEE Power Energy Soc. Gen. Meeting*, Jul. 2017, pp. 1–5.

[32] A. H. Mohamed and K. P. Schwarz, "Adaptive Kalman filtering for INS/GPS," *J. Geodesy*, vol. 73, no. 4, pp. 193–203, May 1999.

[33] C. Campestrini, T. Heil, S. Kosch, and A. Jossen, "A comparative study and review of different Kalman filters by applying an enhanced validation method," *J. Energy Storage*, vol. 8, pp. 142–159, Nov. 2016. [Online]. Available: https://www.sciencedirect.com/science/article/pii/S2352152X16302031

[34] J. Wang, "Stochastic modeling for real-time kinematic GPS/GLONASS positioning," *Navigation*, vol. 46, no. 4, pp. 297–305, Dec. 1999, doi: 10.1002/j.2161-4296.1999.tb02416.x.

[35] B. J. Jonkman, "Turbsim user's guide v2. 00.00," Nat. Renew. Energy Lab., Denver West Parkway Golden, CO, USA, 2014. [Online]. Available: https://www.nrel.gov/wind/nwtc/turbsim.html

[36] J. M. Jonkman and K. Shaler. (2021). *Fast Farm User's Guide and Theory Manual*. National Renewable Energy Laboratory Golden, CO, USA. [Online]. Available: https://openfast.readthedocs.io/en/dev/source/user/fast.farm/index.html

[37] B. Jonkman and J. Jonkman, "Fast v8. 16.00 A-BJJ," Nat. Renew. Energy Lab., Denver West Parkway Golden, CO, USA, Tech. Rep. 1355, 2016. [Online]. Available: https://github.com/openfast

[38] P. Hintjens, *ZeroMQ: Messaging for Many Applications*. Newton, MA, USA: O'Reilly Media, 2013. [Online]. Available: https://github.com/scemama/f77_zmq

[39] J. Jonkman, S. Butterfield, W. Musial, and G. Scott. (Feb. 2009). *Definition of a 5-mW Reference Wind Turbine for Offshore System Development*. [Online]. Available: https://www.osti.gov/biblio/947422

[40] J. N. Kutz, S. L. Brunton, B. W. Brunton, and J. L. Proctor, *Dynamic Mode Decomposition*. Philadelphia, PA, USA: Society for Industrial and Applied Mathematics, 2016, doi: 10.1137/1.9781611974508.

[41] P. Benner, C. Himpe, and T. Mitchell, "On reduced input–output dynamic mode decomposition," 2017, *arXiv:1712.08447*.

MINJEONG KIM received the B.S., M.S., and Ph.D. degrees in aerospace engineering from Sejong University, Seoul, South Korea, in 2016, 2018, and 2023, respectively. She is currently a Postdoctoral Researcher with the Flight Dynamics and Control Laboratory, Sejong University. Her primary research interests include modeling and control of dynamic systems, data analytics, and machine learning.

MINHO JANG received the B.S. degree from the Department of Electrical and Computer Engineering, Chonnam National University, Gwangju, South Korea, in 2021. He is currently pursuing the master's degree in aerospace engineering with Sejong University. His research interest includes optimal control.

SUNGSU PARK received the B.S. and M.S. degrees from Seoul National University, South Korea, and the Ph.D. degree from UC Berkeley. He is currently a Professor of aerospace engineering with Sejong University, Seoul, South Korea. His current research interests include machine learning and optimization applications in guidance, navigation, and control system designs.

• • •